

## Chromatin state dynamics during blood formation

Author(s): David Lara-Astiaso, Assaf Weiner, Erika Lorenzo-Vivas, Irina Zaretsky, Diego Adhemar Taitin, Eyal David, Hadas Keren-Shaul, Alexander Mildner, Deborah Winter, Steffen Jung, Nir Friedman and Ido Amit

Source: *Science*, Vol. 345, No. 6199 (22 AUGUST 2014), pp. 943-949

Published by: American Association for the Advancement of Science

Stable URL: <https://www.jstor.org/stable/10.2307/24917249>

### REFERENCES

Linked references are available on JSTOR for this article:

[https://www.jstor.org/stable/10.2307/24917249?seq=1&cid=pdf-reference#references\\_tab\\_contents](https://www.jstor.org/stable/10.2307/24917249?seq=1&cid=pdf-reference#references_tab_contents)

You may need to log in to JSTOR to access the linked references.

JSTOR is a not-for-profit service that helps scholars, researchers, and students discover, use, and build upon a wide range of content in a trusted digital archive. We use information technology and tools to increase productivity and facilitate new forms of scholarship. For more information about JSTOR, please contact support@jstor.org.

Your use of the JSTOR archive indicates your acceptance of the Terms & Conditions of Use, available at <https://about.jstor.org/terms>



American Association for the Advancement of Science is collaborating with JSTOR to digitize, preserve and extend access to *Science*

JSTOR

construct ( $\Delta rli55$ :Empty) could not prevent expression of the *eut* genes in ethanolamine alone (as in the parental  $\Delta rli55$  strain), whereas a strain with a wild-type copy of *rli55* ( $\Delta rli55$ :*rli55*) fully restored Rli55-mediated inhibition. However, a strain with a deletion in the riboswitch ( $\Delta rli55$ : $\Delta$ ribo) inhibited *eut* expression in all conditions, as the riboswitch can no longer terminate *rli55* transcription in response to  $B_{12}$ . In strain  $\Delta rli55$ :*rli55* $\Delta$ M1, wherein four uridine residues in the first ANTAR site were mutated to adenines (Fig. 3D,  $\Delta$ M1), inhibition of *eut* expression by Rli55 was abolished in the presence of ethanolamine alone. In contrast, in strain  $\Delta rli55$ :*rli55* $\Delta$ M1/M2, where compensatory mutations were made to the opposite side of the ANTAR stem-loop (Fig. 3D,  $\Delta$ M2), wild-type regulation of *eut* expression was restored. Mutation of the six nucleotides in the stem-loop of the second ANTAR element (Fig. 3D,  $\Delta$ M3,  $\Delta rli55$ :*rli55* $\Delta$ M3) had no significant effect on Rli55-mediated regulation. Thus, the first ANTAR element is necessary and sufficient for Rli55-mediated regulation.

The long form of Rli55 containing an ANTAR element might bind and sequester EutV and so prevent it from activating expression of the *eut* genes in the presence of ethanolamine but absence of  $B_{12}$ . When sufficient levels of  $B_{12}$  accumulate,  $B_{12}$  would bind the riboswitch, producing truncated Rli55 transcripts, which would lack an ANTAR element and be unable to sequester EutV. To examine this hypothesis, we constructed a strain with an additional copy of the *eutV* gene carrying a 2XFLAG-tag (EutV<sup>FLAG</sup>) and first showed that expression of EutV<sup>FLAG</sup> protein is regulated identically to the native *eutV* gene in response to ethanolamine and  $B_{12}$  (fig. S6A). We also constructed a strain with an additional *eutV* gene lacking a FLAG tag (EutV<sup>NOFLAG</sup>). Anti-FLAG immunoprecipitations of cell lysates from these two strains (fig. S6, B and C), followed by RNA-seq analysis (Fig. 3, E and F), showed that Rli55 is enriched by coimmunoprecipitation with EutV<sup>FLAG</sup> primarily when bacteria are grown in the presence of ethanolamine alone, although we saw no enrichment in a parallel immunoprecipitation with the EutV<sup>NOFLAG</sup> strain (Fig. 3E). In contrast, the ANTAR element upstream of the *eutV* gene (Fig. 3F) is enriched by coimmunoprecipitation of lysates from EutV<sup>FLAG</sup> bacteria, but not EutV<sup>NOFLAG</sup> bacteria, grown in the presence of ethanolamine and  $B_{12}$  together but not from lysates of bacteria grown in ethanolamine alone. To a lesser extent, the ANTAR-containing region upstream of *eut4* and the entire *eut4*-Q locus are enriched under the latter condition (fig. S7). These data support a model in which the majority of EutV is bound and sequestered by Rli55 in the presence of ethanolamine alone. Conversely, in the presence of ethanolamine and  $B_{12}$ , the riboswitch produces short truncated Rli55 transcripts, which cannot bind EutV, and so allows EutV to bind *eut* mRNAs and to activate *eut* expression (Fig. 3G).

This riboregulatory mechanism coordinates expression of the ethanolamine utilization (*eut*)

locus with the availability of  $B_{12}$ , the essential cofactor for ethanolamine catabolism. Previously, ethanolamine utilization has been shown to be important after oral infection by *Salmonella enterica* serovar Typhimurium and enterohemorrhagic *Escherichia coli* (3, 4, 14); however, the contribution of ethanolamine utilization to *L. monocytogenes* pathogenesis in an intravenous mouse infection model suggests that ethanolamine utilization is important outside of the intestine and possibly in the intracellular environment. This study also extends the role of riboswitches in the regulation of noncoding RNAs (15, 16). Finally, our data show that Rli55 represents a new member of the small family of regulatory RNAs that function by sequestering a protein, which also includes the 6S and CsrB/C RNAs (17), and highlights a distinctive means of signal integration in bacterial gene regulation.

#### REFERENCES AND NOTES

- D. A. Garsin, *Nat. Rev. Microbiol.* **8**, 290–295 (2010).
- K. Koichi, F. Michiya, N. Makoto, *Biochim. Biophys. Acta* **369**, 222–233 (1974).
- P. Thiennimitr et al., *Proc. Natl. Acad. Sci. U.S.A.* **108**, 17480–17485 (2011).
- Y. Bertin et al., *Environ. Microbiol.* **13**, 365–377 (2011).
- O. Tsay, D. Ravcheev, A. Mushegian, *J. Bacteriol.* **191**, 7157–7164 (2009).
- C. Archambaud et al., *Proc. Natl. Acad. Sci. U.S.A.* **109**, 16684–16689 (2012).
- M. F. Del Papa, M. Perego, *J. Bacteriol.* **190**, 7147–7156 (2008).
- K. A. Fox et al., *Proc. Natl. Acad. Sci. U.S.A.* **106**, 4435–4440 (2009).
- J. R. Roth, J. G. Lawrence, T. A. Bobik, *Annu. Rev. Microbiol.* **50**, 137–181 (1996).
- A. Toledo-Arana et al., *Nature* **459**, 950–956 (2009).
- W. C. Winkler, R. R. Breaker, *Annu. Rev. Microbiol.* **59**, 487–517 (2008).
- O. Wurtzel et al., *Mol. Syst. Biol.* **8**, 583 (2012).
- A. Ramesh et al., *PLOS Genet.* **8**, e1002666 (2012).
- S. E. Winter, A. J. Bäumler, *Gut Microbes* **2**, 58–60 (2011).
- J. R. Mellin et al., *Proc. Natl. Acad. Sci. U.S.A.* **110**, 13132–13137 (2013).
- G. André et al., *Nucleic Acids Res.* **36**, 5955–5969 (2008).
- S. Gottesman, G. Storz, *Cold Spring Harb. Perspect. Biol.* **3**, a003798 (2011).

#### ACKNOWLEDGMENTS

We are grateful to D. Garsin and W. Winkler for their exchange of ideas and discussion of unpublished data. We also thank, N. King and J. Pederson for helpful and insightful discussions and Y. Chao and J. Vogel for assistance with the CLIP-seq protocol. This work was supported by grants to P.C., European Research Council advanced grant (233348), ANR (BACNET 09-BLAN-0024-02), ANR Investissement d'Avenir Programme (10-LABX-62), Fondation Le Roch, and Fondation Jeantet. P.C. is an International Senior Research Scholar of the Howard Hughes Medical Institute.

#### SUPPLEMENTARY MATERIALS

[www.sciencemag.org/content/345/6199/940/suppl/DC1](http://www.sciencemag.org/content/345/6199/940/suppl/DC1)  
Materials and Methods  
Figs. S1 to S7  
Tables S1 and S2  
References  
21 April 2014; accepted 24 June 2014  
10.1126/science.1255083

#### IMMUNOGENETICS

## Chromatin state dynamics during blood formation

David Lara-Astiaso,<sup>1\*</sup> Assaf Weiner,<sup>2,3\*</sup> Erika Lorenzo-Vivas,<sup>1</sup> Irina Zaretsky,<sup>1</sup> Diego Adhemar Jaitin,<sup>1</sup> Eyal David,<sup>1</sup> Hadas Keren-Shaul,<sup>1</sup> Alexander Mildner,<sup>1</sup> Deborah Winter,<sup>1</sup> Steffen Jung,<sup>1</sup> Nir Friedman,<sup>2,3†</sup> Ido Amit<sup>1†</sup>

Chromatin modifications are crucial for development, yet little is known about their dynamics during differentiation. Hematopoiesis provides a well-defined model to study chromatin state dynamics; however, technical limitations impede profiling of homogeneous differentiation intermediates. We developed a high-sensitivity indexing-first chromatin immunoprecipitation approach to profile the dynamics of four chromatin modifications across 16 stages of hematopoietic differentiation. We identify 48,415 enhancer regions and characterize their dynamics. We find that lineage commitment involves de novo establishment of 17,035 lineage-specific enhancers. These enhancer repertoire expansions foreshadow transcriptional programs in differentiated cells. Combining our enhancer catalog with gene expression profiles, we elucidate the transcription factor network controlling chromatin dynamics and lineage specification in hematopoiesis. Together, our results provide a comprehensive model of chromatin dynamics during development.

**C** chromatin plays a major regulatory role in cell-type-specific functions and response (1, 2). The current dogma of cellular differentiation suggests that there is a progressive closing of the regulatory potential of the genome. According to this model, differentia-

tion is a gradual transition from an open chromatin state in multipotent stem cells to a compacted chromatin state in differentiated cells. However, genome-wide histone modification profiling of embryonic stem cells and terminally differentiated cells is not fully compatible with this model

(3–7). Resolving this discrepancy requires observation of chromatin dynamics during intermediate stages of differentiation.

An important model system for differentiation is hematopoiesis, in which a single hematopoietic stem cell gives rise to a large number of cell types (comprising the blood) through a series of characterized intermediate progenitor cells (8, 9). Chromatin regulation has a central role in hematopoiesis: Mutations or loss of chromatin factors lead to hematopoiesis defects and diseases (10). Moreover, genome-wide chromatin profiling studies have revealed large-scale differences in the histone modifications and transcription factor binding maps between mature immune cell types (3–6, 11). Thus, dramatic chromatin reorganizations during hematopoiesis are critical for early hematopoietic decisions (12).

Comprehensive study of the chromatin events during hematopoiesis has been hampered by the low sensitivity and reproducibility for small cell numbers with current chromatin immunoprecipitation (ChIP) protocols. These protocols require several enzymatic steps with limited performance when the input DNA is below the nanogram range. Whereas an average diploid mammalian cell has roughly 4 to 8 pg of DNA, losses after ChIP reduce the available DNA for analysis by 2 to 3 orders of magnitude, setting the lower limit for genome-wide chromatin analysis at 50,000 cells (13). Amplification of ChIP material partially alleviates this problem at the cost of introducing amplification biases (14, 15).

To profile chromatin dynamics of scarce *in vivo* cell populations, we developed an indexing-first chromatin IP approach (iChIP). In this protocol, barcoding is performed directly on the total cellular chromatin (Fig. 1A), thereby avoiding the low-input enzymatic reactions occurring in conventional ChIP. Importantly, this enables multiple chromatin-barcoded samples to be pooled for ChIP in the same well, further reducing initial input requirements and increasing cross-sample reproducibility. To minimize centrifugation steps, cells are fixed before sorting and sonication. Then, the sheared chromatin is immobilized on magnetic beads coated with antibody to H3 and then indexed. The indexed chromatin is released from the H3 beads and pooled with chromatin from other samples. Finally, ChIP is performed with the desired antibody, and a single chromatin-barcoded pool can be divided among multiple ChIPs for profiling various chromatin modifications.

The iChIP protocol is highly reproducible for low cell numbers (a few hundred cells) while increasing the sensitivity and throughput (Fig. 1). To benchmark iChIP, we barcoded decreasing amounts (10,000 to 500 cells) of chromatin iso-

lated from bone-marrow-derived dendritic cells (BMDCs), in triplicate, and performed ChIP on the barcoded chromatin with an antibody to mono- and trimethylated histone H3 lysine 4 (H3K4me1 and H3K4me3) (Fig. 1, B to D, and fig. S1). We confirmed reproducibility of H3K4me3 peaks between replicates of 10,000 cells ( $r = 0.95$ ) down to 500 cells ( $r = 0.85$ ). iChIP profiles correlated with conventional ChIP-seq on 10 million BMDCs ( $r = 0.92$ ) (16). iChIP is applicable to profile other histone modifications and transcription factors for low cell numbers (Fig. 1, C and D, and fig. S1). The reproducibility and sensitivity for small cell numbers of iChIP open the way for *in vivo* characterization of chromatin dynamics during hematopoiesis.

We profiled four histone modifications (H3K4me1, H3K4me2, H3K4me3, and H3K27ac) (17) in three *in vivo* replicates at 16 developmental stages of hematopoietic commitment using 5000 cells per mark. The cell populations chosen comprise all multipotent progenitor stages and the common lineage oligopotent progenitors from each of the major blood lineages (myeloid, lymphoid, and erythroid), as well as several terminally differentiated cell types from each of the lineages (<https://www.immgen.org>) (16) (Fig. 2A). Replicates of histone modifications ChIP and RNA-seq displayed high reproducibility [average  $r = 0.95$ ] (fig. S2 and tables S1 and 2). We used histone marks to define promoter (high H3K4me3) and enhancer (high H3K4me1/2 and low H3K4me3) regions, resulting in analysis of 48,415 enhancers and 17,923 promoters (16). Enhancer activity was defined from H3K27ac levels and RNA expression values of the nearest gene (16–18). Genome-wide analysis of RNA expression and promoter activity (H3K4me3 signal) identified four major patterns for progenitor, lymphoid, myeloid, and erythroid cells (Fig. 2B and figs. S2 and S3). In contrast, H3K4me1 signal revealed that lineage progenitors were more similar to the differentiated cells within their lineage than to progenitors from other cell lineages (Fig. 2B and figs. S2 and S3). This distinction suggests that enhancer establishment is initiated in early lineage commitment and can reveal the differentiation potential of progeny before the execution of the RNA expression program.

Changes in chromatin marks during hematopoiesis (particularly H3K4me1 and H3K4me2) suggest lineage-specific activity of regulatory elements. Of the 48,415 hematopoietic enhancers, 90% (43,428) changed state during hematopoiesis (16). We found that 60% (26,393) of these dynamic enhancers show the stereotypical behavior in which they are initially marked in hematopoietic stem cells (HSCs) but are maintained only in the relevant lineage [Fig. 2C (Gata2) and fig. S4A (Meis1 and CD34)]. Surprisingly, we discovered that a large proportion of dynamic enhancers (40%, 17,035) are established *de novo* during the differentiation process (16). For example, enhancers present in myeloid gene loci IL-1b, CD14, S100a8, and F7 (coagulation factor VII) are either established *de novo* or become more prominent in the myeloid lineage

(Fig. 2C and fig. S4A). Similarly, Ebf1 and Cr2 enhancers are established in B cells; Bcl1b and CD3g enhancers in T cells; Granzyme A and Ncr1 enhancers in natural killer cells (NK) cells; and Gata1, Gypa (glycophorin A), and Cpxo (coproporphyrinogen oxidase) enhancers in the erythroid lineage (Fig. 2 and figs. S3B and S4A).

The establishment of *de novo* lineage-specific enhancers occurs mainly at the root of the commitment point in the first progenitor of the lineage, whereas closing of enhancers occurs more gradually (Fig. 2). For example, S100a8, F7 and F10 loci display H3K4me1 signal specifically in the myeloid lineage, with *de novo* establishment of the enhancers at the root of the myeloid commitment point in common myeloid progenitor (CMP) (Fig. 2C and figs. S3B and S4A). Similarly, the Cpxo and Gypa loci display H3K4me1 signal specifically in the erythrocyte lineage, with *de novo* establishment of the enhancers at the root of the erythrocyte commitment point in the megakaryocyte erythroid progenitor (MEP) (Fig. 2C). Importantly, we observe a stepwise acquisition of the different chromatin modifications in the lineage-specific enhancers during hematopoiesis (Fig. 2D and figs. S4B and S5). For example, in both S100a8 (myeloid lineage) and Gypa (erythroid lineage) loci, H3K4me1/2 appear first in the root lineage progenitor (CMP and MEP, respectively), whereas H3K27ac (locus activation) is acquired together with active RNA transcription only once the cells (granulocytes and erythrocyte B) are terminally differentiated (Fig. 2D and fig. S4B). Globally, 32% of the activated (H3K27ac) enhancers in terminally differentiated cells are initially poised (H3Kme1 only) in the lineage progenitors (16).

Clustering of all 48,415 H3K4me1 peaks by their dynamic profiles during hematopoiesis revealed nine major clusters, consistent with the underlying biology of the system (Fig. 3A and fig. S6, A and B) (16). H3K4me2 signal shows similar patterns in all nine clusters (fig. S6A). Cluster I comprises enhancers shared throughout hematopoiesis. Clusters II to IV group lineage-specific enhancers already marked in HSCs and shared with hematopoietic progenitors. Finally, clusters VI (Fig. 3B, middle), VII, VIII, and IX (Fig. 3B, bottom) group *de novo* enhancers that are specific to a particular lineage and were not marked in HSCs with 6382 myeloid, 5834 lymphoid, and 4819 erythroid enhancers. We also found a group of 6612 enhancers (cluster V) shared exclusively among progenitors (Fig. 3B, top). Interestingly, the erythrocyte and progenitor enhancer clusters exhibit relatively high sequence conservation (16) in the mammalian clade, with the myeloid and lymphoid enhancers displaying lower conservation. These data suggest differential rates of evolutionary dynamics in these cis-regulatory regions (16) (Fig. 3A).

Newly formed enhancers could either be established at a specific branching point or established gradually during the development process. To further examine these dynamics, we generated a catalog of enhancers that are dynamic (gained or lost) during the process of differentiation from

<sup>1</sup>Department of Immunology, Weizmann Institute of Science, Rehovot, Israel. <sup>2</sup>Institute of Life Sciences, The Hebrew University, Jerusalem, Israel. <sup>3</sup>School of Computer Science and Engineering, The Hebrew University, Jerusalem, Israel.

\*These authors contributed equally to this work. †Corresponding author. E-mail: nir.cs.huji.ac.il (N.F.); ido.amit@weizmann.ac.il (I.A.)

the long-term hematopoietic stem cells (LT-HSCs) to mature, terminally differentiated cells (Fig. 3C). We determined, for each enhancer, the stage of gain or loss along the differentiation path. In erythroid differentiation, 65% of the de novo

enhancer repertoire are gained in the MEP stage (Fig. 3D). Similarly, 40 to 50% of the de novo myeloid enhancers are gained in the first step of myeloid commitment, during the multipotent progenitor (MPP) to CMP transition,

whereas the CMP to GMP transition involves fewer gains (15 to 30%). Together, the CMP and GMP stages are responsible for 63 to 80% of gained enhancers in terminally differentiated myeloid cells (Fig. 3D), consistent with the global

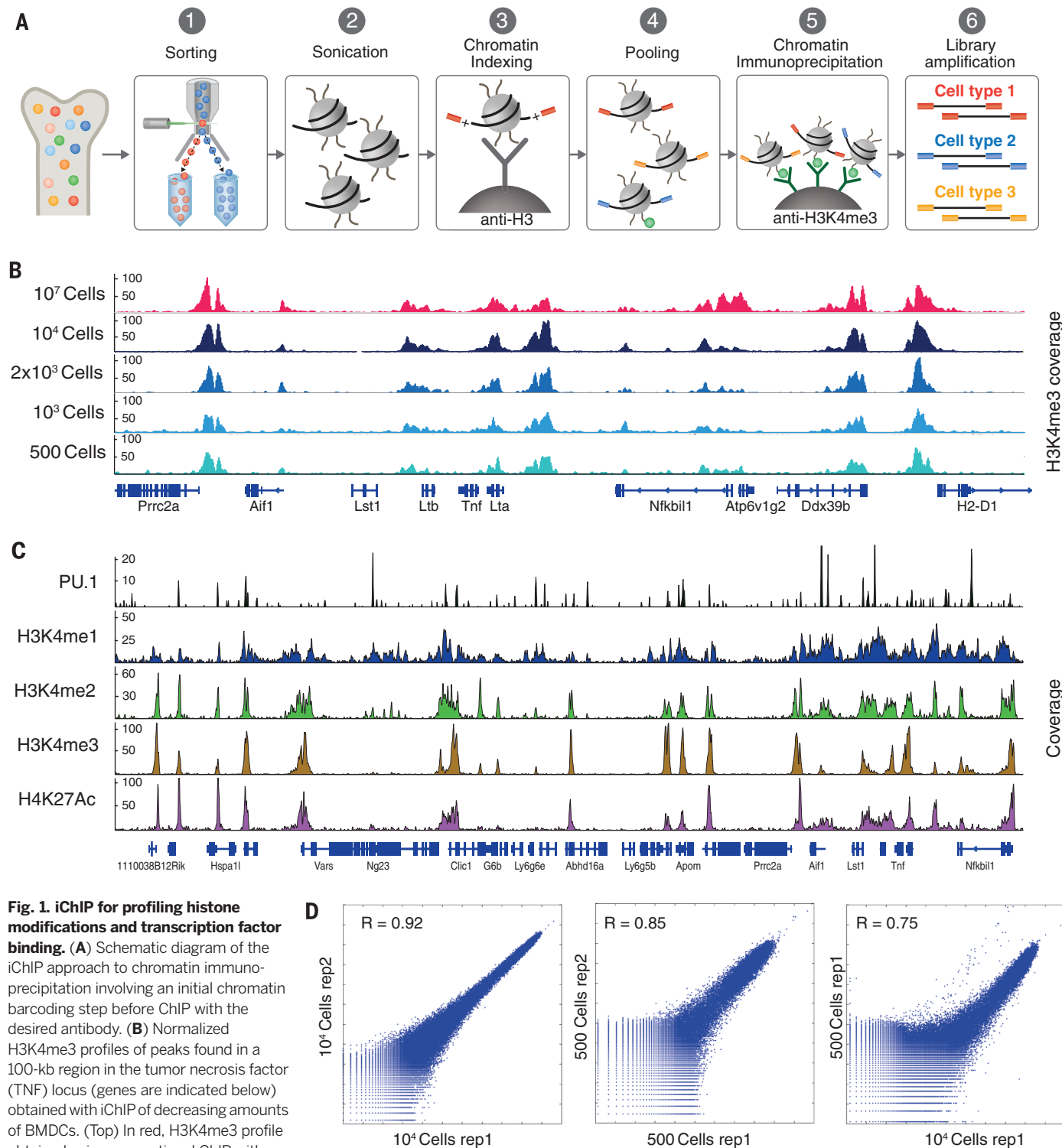


**Fig. 1. iChIP for profiling histone modifications and transcription factor binding.** (A) Schematic diagram of the iChIP approach to chromatin immunoprecipitation involving an initial chromatin barcoding step before ChIP with the desired antibody. (B) Normalized H3K4me3 profiles of peaks found in a 100-kb region in the tumor necrosis factor (TNF) locus (genes are indicated below) obtained with iChIP of decreasing amounts of BMDCs. (Top) In red, H3K4me3 profile obtained using conventional ChIP with 20 million cells (15). Below, in shades of blue, H3K4me3 profiles obtained with iChIP. (C) Normalized profiles of PU.1, H3K4me1, H3K4me2, H3K4me3, and H3K27ac found in a 250-kb region in the TNF locus obtained with iChIP with  $10^4$  BMDCs. (D) Scatter plots showing correlation between representative H4Kme3 iChIP replicates. From left to right: correlation between  $10^4$  cell replicates, 500 cell replicates, and 500 cells compared with  $10^4$  cells.

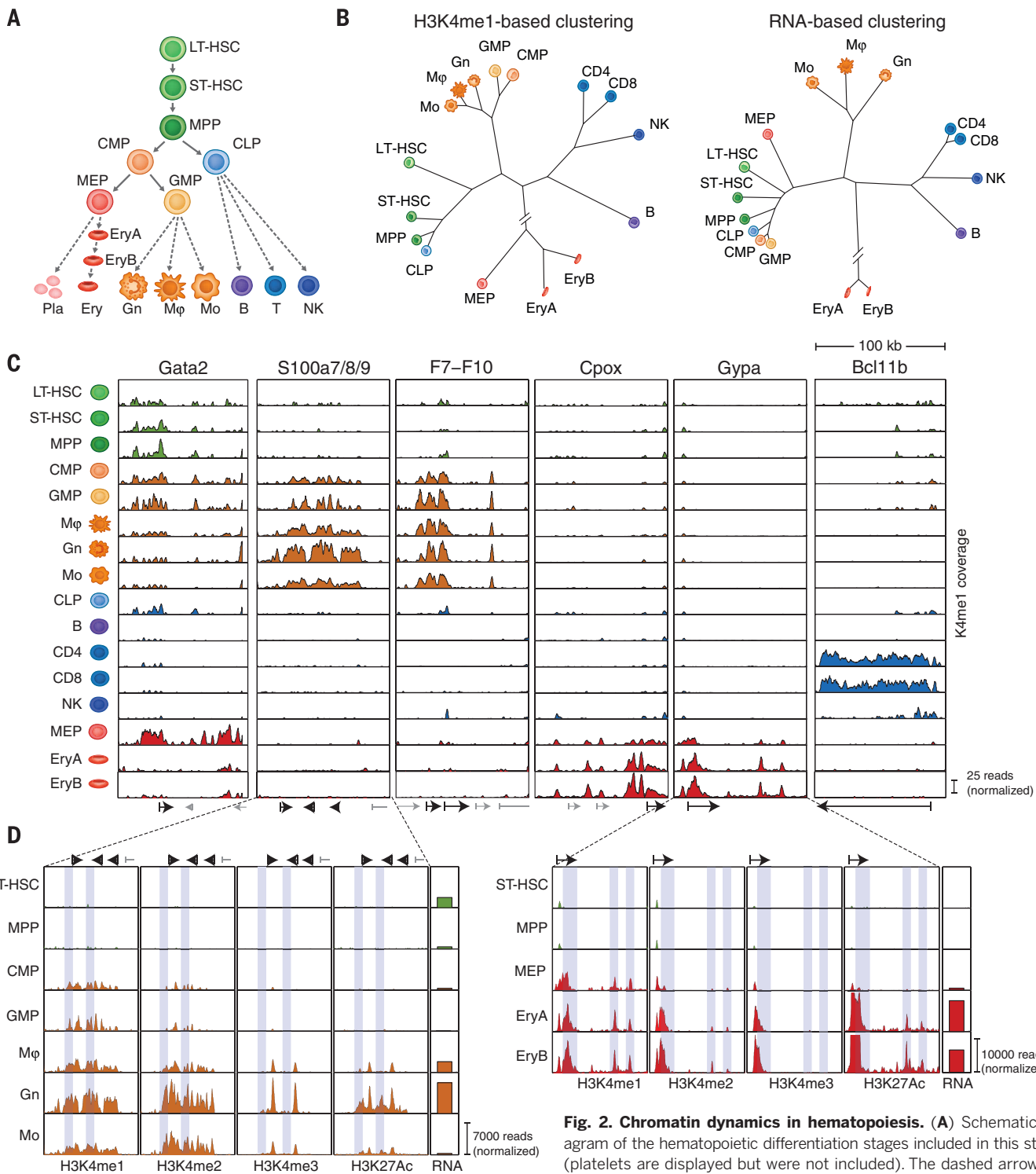


**Fig. 2. Chromatin dynamics in hematopoiesis.** (A) Schematic diagram of the hematopoietic differentiation stages included in this study (platelets are displayed but were not included). The dashed arrow indicates intermediate progenitors not measured in this study. Color code:

green for multipotent progenitors, orange for myeloid lineage (including the oligopotent progenitors CMP and GMP), blue for lymphoid lineage, and red for erythroid lineage. (B) Clustering dendrogram of cell types based on H3K4me1 profiles (left) and RNA-seq levels (right) showing the differential association of lineage progenitors (CMP, GMP, and MEP). (C) Representative examples of H3K4me1 signal (cell types labeled at left) in several loci (from left to right): Gata2 for progenitors, F7-F10 and S100a8 for myeloid lineage, Gypa and Cpox for erythroid lineage, and Bcl11b for T cells. Displayed are normalized reads coverage in a 100-kb region around the gene body. (D) Profiles of H3K4me1, H3K4me2, H3K4me3, and H3K27ac modifications and RNA expression levels in two lineage-specific gene loci: S100a8 (myeloid) and Gypa (erythroid). Displayed are profiles for the lineage-specific cell types and multipotent progenitor cells over a 100-kb region around the gene body. Putative lineage-specific enhancers are shadowed in blue. Lineage-specific genes are indicated below (black), as well as other genes in the loci (light gray).

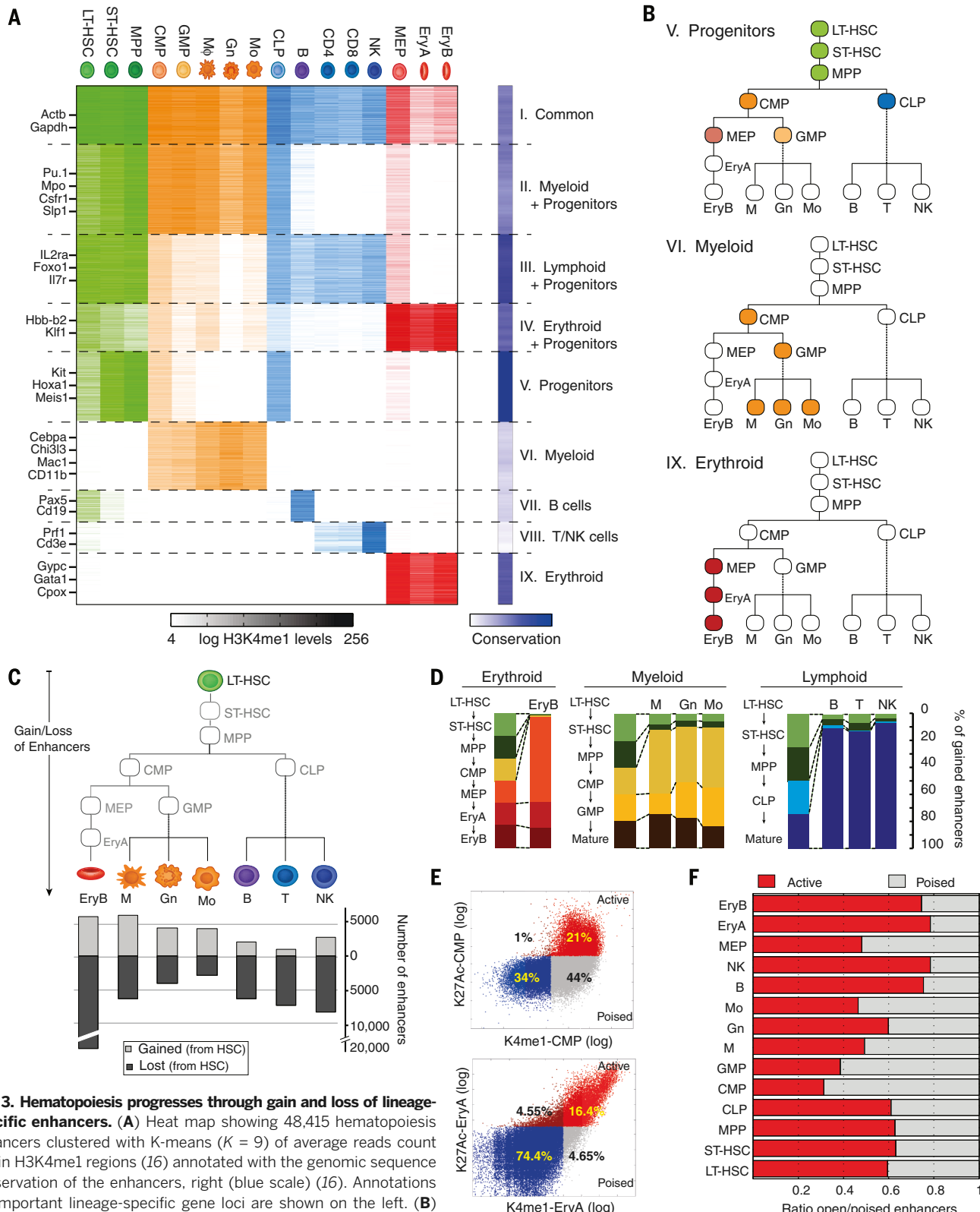


**Fig. 3. Hematopoiesis progresses through gain and loss of lineage-specific enhancers.** (A) Heat map showing 48,415 hematopoiesis enhancers clustered with K-means ( $K = 9$ ) of average reads count within H3K4me1 regions (16) annotated with the genomic sequence conservation of the enhancers, right (blue scale) (16). Annotations for important lineage-specific gene loci are shown on the left. (B) Schematic tree view of three representative enhancer clusters: progenitors (V), myeloid (VI), and erythroid (IX). Color fill represents stages with H3K4me1 mark at the enhancer. (C) Bar plot showing the number of enhancers gained (top, light gray) and lost (bottom, dark gray) during the development from HSC to mature hematopoietic cells along each lineage. (D) Bar plot showing the percent of de novo enhancers [from (C)] established at each developmental stage from HSC to mature hematopoietic cells.

(E) Scatter plots showing H3K27ac signal versus H3K4me1 signal in both CMPs and EryA cells. Active enhancers (H3K4me1 positive and H3K27ac positive) are colored in red, poised enhancers (H3K4me1 positive and H3K27ac negative) in light gray, and inactive enhancers (H3K4me1 negative and H3K27ac negative) in blue. (F) Proportions of active (red) and poised (light gray) enhancers in each of the cell types studied.

**Fig. 4. Lineage-specific enhancers are associated with transcription factor cohorts.**

(A) ATAC-seq signal co-occurs temporally with H3K4me1 in lineage-specific enhancers. Shown are normalized profiles in nine hematopoietic cells for ATAC-seq (black) and H3K4me1 in erythroid-specific Gypa (red) and myeloid-specific F7-10 loci (orange). Displayed are peaks found in a 100-kb region around the gene body. Putative enhancers (K4me1) shadowed in blue; transcriptional start site shadowed in red. Enlargement of ATAC-seq peak is shown below.

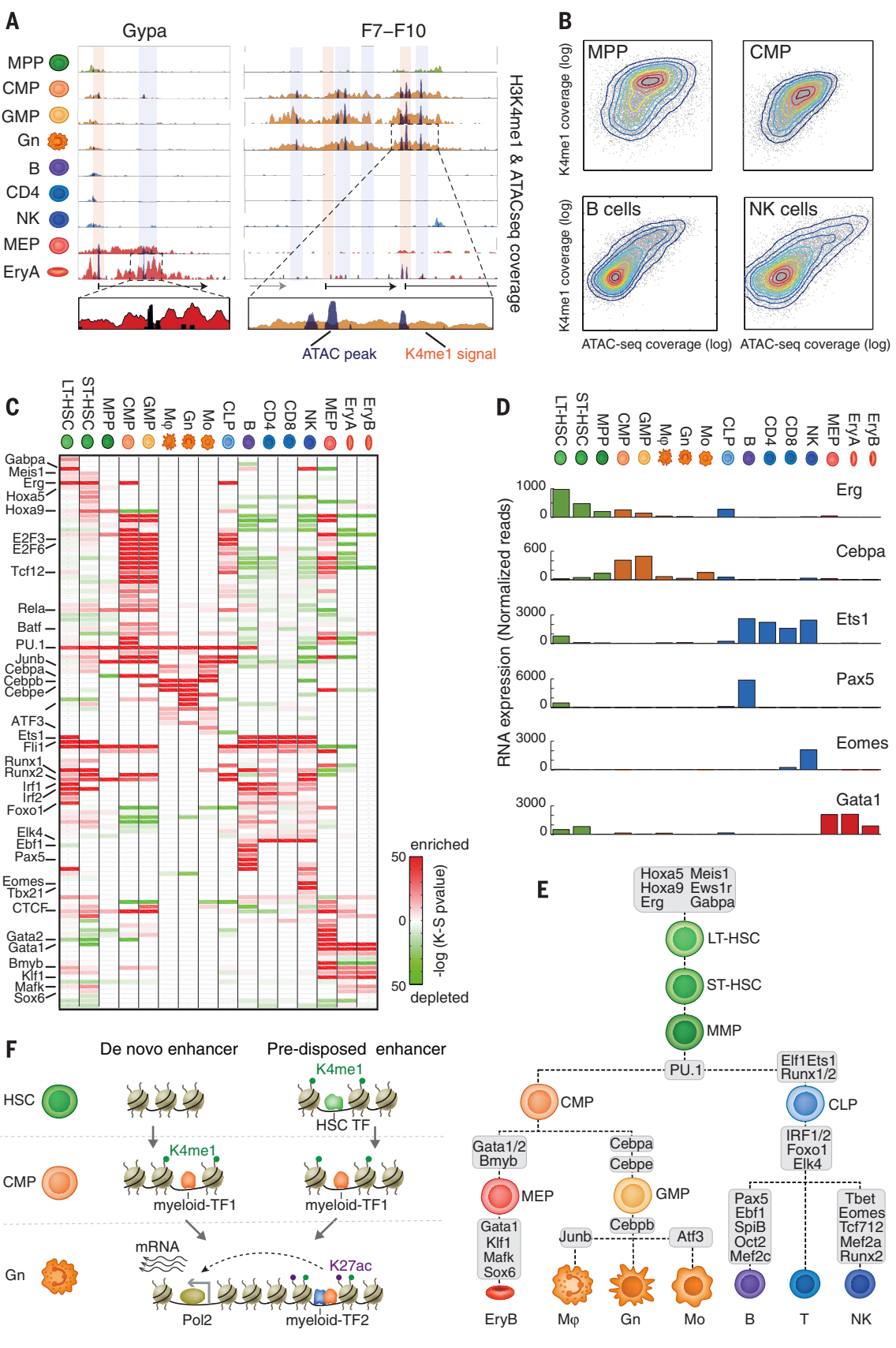
(B) Scatter plot showing correlation between H3K4me1 signal and enhancer-restricted ATAC-seq signal in four cell types: B cells, NK cells, MPPs, and CMPs (colors represent density or points).

(C) Heat map showing the *P* values of transcription factor motif (Kolmogorov-Smirnov test) for the indicated cell-type-specific enhancers (16). Red indicates significant enrichment ( $P < 1 \times 10^{-5}$ ) of motif associated to the labeled transcription factor; green indicates motif depletion ( $P < 1 \times 10^{-5}$ ). White indicates either no significant enrichment or no RNA expression.

(D) Bar plots showing gene expression profiles across the hematopoietic cell types for representative transcription factors [from (C)].

(E) Schematic of the hematopoietic tree showing the representative transcription factors regulating the lineage enhancers at each cell type as predicated by the logistic model.

(F) Schematic of establishment of lineage-specific enhancers in the myeloid lineage by a conventional mechanism (right) as well as through transcription factor-mediated establishment of de novo enhancers (left).



enhancer similarity of CMP and GMP with the myeloid lineage (Fig. 2B). In contrast, enhancer loss is a more gradual process that initiates in the CMP or MEP stage (for myeloid and erythrocyte development, respectively) with a large proportion (40 to 50%) of enhancers lost in the last and definitive differentiation step to mature cells (fig. S6C).

Genome-wide studies show that, whereas H3K4me1 marks both poised and active enhancers, H3K27ac marks only active enhancers (19, 20). Because poised enhancers represent potential gene expression programs, the ratio of these enhancers in a given cell type approximates the current regulatory potential of the cell (20). Analysis of the regulatory potential in hematopoiesis shows that progenitor cells are more plastic than differentiated cell types, with erythrocytes using most (78%) of their enhancers, whereas CMPs use only 33% of their enhancer potential (Fig. 3, E and F, and fig. S6D) (16). Within the progenitor group, CMP and GMP are more plastic than the multipotent stem cells (33 to 37% versus 62 to 65% of enhancer use), likely due to the de novo expansion of myeloid enhancers (Fig. 2B and Fig. 3, A and F). Notably, there is a wide spectrum of plasticity across the terminally differentiated cells, with the myeloid lineage (macrophages, monocytes, and granulocytes) showing higher degrees of plasticity than erythrocytes, B cells, and NK cells; this is consistent with the higher functional versatility of myeloid cells in comparison with other hematopoietic cell types (21).

De novo H3K4me1 establishment in hematopoiesis is concomitant to an increase in chromatin accessibility (Fig. 4, A and B). We measured chromatin accessibility, “open chromatin” (22), during the developmental process in 10 hematopoietic cell types using the assay for transposase-accessible chromatin followed by sequencing (ATAC-seq) (23). In erythroid (Gypa) and myeloid (F7 and F10) gene loci, chromatin accessibility follows the temporal pattern observed for H3K4me1 (Fig. 4A). As expected, the ATAC signal is enriched both in active promoters and H3K4me1-positive enhancers, as well as in insulators and other regulatory regions (23). To evaluate the proportion of de novo enhancers that also display de novo establishment of open chromatin, we plotted the ATAC-seq signal in the regions from the H3K4me1 enhancer catalog (fig. S7A). We compared the ATAC-seq signal to H3K4me1 and H3K27ac intensities. We observed a similar pattern between ATAC and H3K4me1 signal ( $r = 0.75$ ) and a weakened agreement with H3K27ac ( $r = 0.62$ ) (Fig. 4B and fig. S7B), suggesting that the process of gain or loss of H3K4me1 mark on enhancers occurs concomitantly with formation of open chromatin sites.

Establishment of lineage-specific enhancers is regulated by the activity of lineage-specific transcription factors (24) (Fig. 4, C to E). Using the ATAC peaks (16) and our enhancer catalog, we searched for enriched transcription factor binding motifs in each cell type (Fig. 4C and fig. S8) (16) to identify lineage-determining fac-

tors. We found that, in line with their identified functions, PU.1, Gata1, and Foxo1 can be classified as potential regulators of myeloid, erythroid, and lymphoid enhancers, respectively (3, 11, 25, 26).

To systematically identify potential regulators, we generated a logistic regression model to predict enhancer activity at each stage from the DNA binding motif scores and transcription factor expression (Fig. 4, D and E, and figs. S8 to S11) (16). Our logistic model accurately predicts enhancer cell-type-specific activity with 75% accuracy (with 70% sensitivity and 80% specificity) (fig. S10B). Importantly, the model allowed us to elucidate the transcription factors controlling chromatin dynamics and lineage specification in hematopoiesis (25, 26). Our model identified the known myeloid lineage determining factors PU.1, Cebpb, and Cebpa as regulators of myeloid enhancers; additionally, our model suggests a hierarchy between the Cebp factors, with Cebpa active in the progenitors (CMP/GMP) and Cebpb replacing Cebpa in the differentiated cell types (Fig. 4E and fig. S11C). Similarly, we identify Meis1, Hoxa9, and Erg as potential regulators of stem cell enhancers; Pax5 in B cells; Klf1 in erythroid cells; and Ets1 in lymphoid cells (Fig. 4, C to E, and fig. S11). We identify many transcription factors that have been implicated in lineage development but have not previously been associated with chromatin regulation of lineage determination, such as Irf1 and Irf2 in B cells and Cebpe in granulocytes (27, 28). We also highlight new potential regulators of hematopoietic lineages: ATF3 in monocytes and Tcf7l2, Mef2a, and Runx2 in NK cells (Fig. 4E). All together, our findings show that chromatin is highly dynamic during hematopoiesis, orchestrated by a defined set of transcription factors.

In conclusion, iChIP enables the execution of reproducible and sensitive ChIP on only a few hundred cells in a manner broadly applicable across organisms and tissues. We show that poised enhancers are established in lineage progenitors before their activation and precede RNA expression in subsequent lineage differentiation. These enhancers are established concomitantly with the formation of open chromatin sites. We then show that most of the enhancer dynamics can be accounted for by the activity of known lineage-specific factors as well as new candidate regulators. These results suggest a new model for chromatin dynamics during differentiation (Fig. 4F) and show that development involves massive dynamic reorganization of the chromatin landscape. Whereas some enhancers are preset in hematopoietic stem cells, as suggested by the conventional development model, a comparable number of enhancers appear to be established de novo during hematopoiesis. We believe that the establishment of newly poised enhancers in the early lineage commitment steps initiates regulatory programs that are subsequently applied in differentiated cells, whereas the closing of enhancers occurs during later differentiation stages. This suggests that cellu-

lar enhancer potential reaches its maximum not at the HSC stage but during the oligopotent progenitor stages. Taken together, these observations reshape our understanding of the role of chromatin and pioneer factors during differentiation.

## REFERENCES AND NOTES

1. L. Ho, G. R. Crabtree, *Nature* **463**, 474–484 (2010).
2. V. W. Zhou, A. Goren, B. E. Bernstein, *Nat. Rev. Genet.* **12**, 7–18 (2011).
3. S. Ghisletti *et al.*, *Immunity* **32**, 317–328 (2010).
4. E. M. Mercer *et al.*, *Immunity* **35**, 413–425 (2011).
5. G. Wei *et al.*, *Immunity* **30**, 155–167 (2009).
6. R. Revilla-i-Domingo *et al.*, *EMBO J.* **31**, 3130–3146 (2012).
7. T. S. Mikkelsen *et al.*, *Nature* **448**, 553–560 (2007).
8. J. Seita, I. L. Weissman, *Wiley Interdiscip. Rev. Syst. Biol. Med.* **2**, 640–653 (2010).
9. S. Doulatov, F. Notta, E. Laurenti, J. E. Dick, *Cell Stem Cell* **10**, 120–136 (2012).
10. A. H. Shih, O. Abdel-Wahab, J. P. Patel, R. L. Levine, *Nat. Rev. Cancer* **12**, 599–612 (2012).
11. S. Heinz *et al.*, *Mol. Cell* **38**, 576–589 (2010).
12. H. Ji *et al.*, *Nature* **467**, 338–342 (2010).
13. T. S. Furey, *Nat. Rev. Genet.* **13**, 840–852 (2012).
14. P. Shankaranarayanan *et al.*, *Nat. Methods* **8**, 565–567 (2011).
15. M. Garber *et al.*, *Mol. Cell* **47**, 810–822 (2012).
16. Materials and methods are available as supplementary materials on Science Online.
17. C. M. Rivera, B. Ren, *Cell* **155**, 39–55 (2013).
18. M. U. Kaikkonen *et al.*, *Mol. Cell* **51**, 310–325 (2013).
19. A. Rada-Iglesias *et al.*, *Nature* **470**, 279–283 (2011).
20. M. P. Creighton *et al.*, *Proc. Natl. Acad. Sci. U.S.A.* **107**, 21931–21936 (2010).
21. T. A. Wynn, A. Chawla, J. W. Pollard, *Nature* **496**, 445–455 (2013).
22. R. E. Thurman *et al.*, *Nature* **489**, 75–82 (2012).
23. J. D. Buenrostro, P. G. Giresi, L. C. Zaba, H. Y. Chang, W. J. Greenleaf, *Nat. Methods* **10**, 1213–1218 (2013).
24. L. A. Cirillo *et al.*, *Mol. Cell* **9**, 279–289 (2002).
25. A. B. Cantor, S. H. Orkin, *Oncogene* **21**, 3368–3376 (2002).
26. W. Ouyang, M. O. Li, *Trends Immunol.* **32**, 26–33 (2011).
27. T. Matsuyama *et al.*, *Cell* **75**, 83–97 (1993).
28. R. Yamanaka *et al.*, *Proc. Natl. Acad. Sci. U.S.A.* **94**, 13187–13192 (1997).

## ACKNOWLEDGMENTS

We thank members of the Amit and Friedman laboratories for critical discussions. We thank G. Brodsky for artwork. This work was supported by grants from the European Research Council (nos. 309788 and 340712), the Israeli Science Foundation (1782/11), the Human Frontier Science Program, Career Development Award (CDA00028/2011-c) (I.A.), a European Molecular Biology Organization Young Investigator Award (I.A.), the National Human Genome Research Institute Center for Excellence in Genome Science (1P50HG006193), and the Israeli Centers of Research Excellence (I-CORE). RNA-seq, ChIP-seq, and ATAC-seq data are deposited in the Gene Expression Omnibus under accession number GSE60103. The data can be viewed from the following Web site: <http://compbio.cs.huji.ac.il/blood-chromatin/index.html>. A patent application for iChIP has been filed by Yeda, Weizmann Institute of Science, Israel.

## SUPPLEMENTARY MATERIALS

[www.sciencemag.org/content/345/6199/943/suppl/DC1](http://www.sciencemag.org/content/345/6199/943/suppl/DC1)  
Materials and Methods  
Figs. S1 to S13  
Tables S1 to S4  
Reference (29, 30)

19 May 2014; accepted 28 July 2014  
Published online 7 August 2014;  
10.1126/science.1256271